Inorganica Chimica Acta 362 (2009) 4553–4562

Contents lists available at ScienceDirect

Inorganica Chimica Acta

journal homepage: www.elsevier.com/locate/ica

A series of cyanide-bridged binuclear complexes

Michael T. Mock [a], Matthew T. Kieber-Emmons [a], Codrina V. Popescu [b], Patrick Gasda [b], Glenn P.A. Yap [a], Charles G. Riordan [a,*]

[a] Department of Chemistry and Biochemistry, University of Delaware, Brown Laboratory, Newark, Delaware 19716, United States
[b] Department of Chemistry, Ursinus College, Collegeville, Pennsylvania 19426, United States

ARTICLE INFO

Article history:
Received 10 February 2009
Accepted 13 May 2009
Available online 27 May 2009

Dedicated to our friend and former colleague, Swiatoslav 'Jerry' Trofimenko.

Keywords:
Cyanide
Cyanide-bridged
Binuclear complex
Linkage isomers
Tp

ABSTRACT

A series of cyanide-bridged binuclear complexes, ('S_3')Ni–CN–M[Tp^{tBu}] ('S_3' = bis(2-mercaptophenyl)sulfide, Tp^{tBu} = hydrotris(3-*tert*-butylpyrazolyl)borate, M = Fe (**2-Fe**), Co (**2-Co**), Ni (**2-Ni**), Zn (**2-Zn**)) was prepared by the coupling of K[('S_3')Ni(CN)] with [Tp^{tBu}]MX. The isostructural series of complexes was structurally and spectroscopically characterized. A similar coupling strategy was used to synthesize the anionic copper(I) analogue, Et_4N{('S_3')Ni–CN–Cu[Tp^{tBu}]}, **2-Cu**.

An alternative synthesis was devised for the preparation of the linkage isomers of **2-Zn**, i.e. of cyanide-bridged linkage isomers. X-ray diffraction, ^{13}C NMR and IR spectral studies established that isomerization to the more stable Ni–CN–Zn isomer occurs. DFT computational results buttressed the experimental observations indicating that the cyanide-bridged isomer is ca. 5 kcal/mol more stable than its linkage isomer.

1. Introduction

Transition metal cyanide complexes have been subject of intense research due to their interesting physical properties including magnetism, color, conductivity and hydrogen storage capacity [1,2]. For example, variations of one of the earliest coordination compounds, Prussian blue, ($[Fe_4\{Fe(CN)_6\}_3]\cdot xH_2O$), has been used to construct room temperature organometallic magnets [3]. Despite the novel physical properties that many transition metal–cyanide complexes exhibit, simple M–CN–M′ complexes containing only one cyanide linkage remain less uncommon. As a consequence, the vibrational properties of such an isolated linkage are not well understood [4] and are worthy of study. In fact, recent reports have focused on fundamental vibrational spectra of M–CN and M–CN–M′ type binding modes, specifically, to understand the spectroscopic differences between CN and the isoelectronic CO ligand [4,5].

Recently, transition metal cyanide motifs have also been revealed as integral components of metalloenzyme active sites. For example, both Ni–Fe and Fe-only hydrogenases, enzymes that catalyze the reversible oxidation of H_2, contain terminal cyanide and carbonyl ligands ligated to the iron center of the active site [6]. Furthermore, cyanide often inhibits or inactivates enzyme catalysis by binding to the enzyme active site(s) in a competitive fashion, i.e. binding at the substrate site. For example, cytochrome *c* oxidase is the target of cyanide poisoning in higher organisms [7]. Inhibitor binding often alters the spectroscopic characteristics of the enzymes, such that these spectroscopic changes can be used as probes providing mechanistic insight concerning the location of inhibitor ion/substrate binding.

Of particular interest in this laboratory is a class of metalloenzymes found in anaerobic bacteria and archaea, carbon monoxide dehydrogenases (COdHs) and acetyl coenzyme A synthase [8]. These metalloenzymes catalyze the interconversion of CO and CO_2 and the synthesis of acetyl coenzyme A, respectively. Crystallographic studies have shown the C-cluster of COdHs from anaerobes contain a $NiFe_3S_4$ cubane subunit ligated to an external single iron site by a bridging cysteine [9], μ-sulfido [10] or hydroxo [11] ligand. Cyanide, a known inhibitor of COdH [12], has been proposed to inhibit by bridging between the nickel and the unique iron [13]. In the proposed catalytic mechanism [14], which finds support in recent crystallographic studies [11], CO binds to the Ni site of the cubane and is attacked by a substrate hydroxide ion that was formally bridging the Ni and unique Fe sites. Hydroxide attack leads to the formation of a Ni-bound carboxylate that subsequently dissociates as CO_2 completing the catalytic cycle. Cyanide was found to displace substrate hydroxide, leading to the suggestion that these anions bind to the same site. This hypothesis raises important questions regarding the role and identity of the bridging ligand in enzyme structure and catalysis. To address these issues, we sought to prepare synthetic complexes that contain a single cyanide bridge between iron and nickel. Whereas there are examples of polycyanide complexes containing a

---

* Corresponding author. Tel.: +1 302 831 1073; fax: +1 509 463 3815.
E-mail address: riordan@udel.edu (C.G. Riordan).

0020-1693/$ - see front matter © 2009 Elsevier B.V. All rights reserved.
doi:10.1016/j.ica.2009.05.042

Ni–NC–Fe linkage [15], we are unaware of either a monocyanide complex containing this bridge or any example of the linkage isomer, Ni–CN–Fe[1]. Herein, we detail binuclear metal complexes containing a single cyanide bridge aimed at modeling inhibited forms of COdH, so as to provide structural and spectroscopic information applicable for analysis of the more complex active site.

2. Experimental

2.1. General procedures

All air and moisture sensitive reactions were performed under N_2 using standard Schlenk line techniques or carried out under an argon or N_2 atmosphere in a Vacuum Atmospheres glovebox equipped with a gas purification system [16]. Unless described otherwise, all reagents were purchased from commercial sources and were used as received. Solvents were dried by passage through activated alumina [17], sparged with N_2, and tested with Na/benzophenone before use. Deuterated solvents and were purchased from Cambridge Isotope Laboratories and stored over 4 Å molecular sieves. $K^{13}CN$ was purchased from Cambridge Isotope Laboratories. KCN and Et_4NCl were purchased from Acros Chemical Company. ‘S_3’–H_2 [18], Tl[Tp^{tBu}] [19], NMe_4[Ni(‘S_3’)(CN)] [18], [Tp^{tBu}]MX (M = Fe, Co, Ni, Zn; X = Cl, Br, I) [19] [Tp^{tBu}]Cu($NCCH_3$) [20], [PhTt^{tBu}]Cu($NCCH_3$) [21], and [Ni(‘S_3’)]$_2$ [18] and were prepared following the published procedures. [Tp^{tBu}]Zn(CN) [22] and its ^{13}CN isotopomer were prepared following the procedure published [19] for the synthesis of [Tp^{tBu}]Zn(N_3) replacing NaN_3 with KCN (or $K^{13}CN$).

^1H and ^{13}C NMR spectra were recorded on a Bruker AC-250, AM-360, DRX-400 or AV-400 MHz NMR spectrometers. NMR spectra were referenced to residual protio solvent signals at ambient temperature unless noted otherwise. NMR abbreviations are as follows: s, singlet; d, doublet; t, triplet; q, quartet; m, multiplet; br, broad. ^{31}P NMR spectra were recorded on either a Bruker DRX-400 or AV-400 MHz NMR spectrometer using an aqueous solution of 85% phosphoric acid in D_2O as an external reference (0 ppm). Solid-state magnetic moments were determined on a Johnson Matthey magnetic susceptibility balance. The magnetic susceptibility of the sample was adjusted for diamagnetic contributions using Pascal's constants. Mössbauer spectra were collected on a spectrometer with closed cycle refrigeration, model CCR4K, operating between 4.5 and 325 K, in constant acceleration mode. The spectrometer was fitted with a permanent 0.3 Tesla magnet. The spectra were analyzed using the software package WMOSS (Dr. Thomas Kent, SEE Co., Minnesota.) Isomer shifts are quoted with respect to iron metal at room temperature. Perpendicular mode, X-band EPR spectra were recorded at 9.44 GHz on a Bruker EMX spectrometer equipped with a ER073 magnet, T103 resonator cavity, ER041MR microwave bridge and ER081 power supply. Sample temperature was controlled by an Oxford Systems LHe cryostat system. Infrared spectra were recorded on a Mattson Genesis Series FTIR spectrometer at ambient temperature and under a purge stream of nitrogen. Solid-state FT-IR samples were prepared as KBr pellets. Cyclic voltammetry was performed in a Vacuum Atmospheres MO–40 M glovebox under an argon atmosphere using a BAS (Bioanalytical Systems) CV–50 W voltammetric analyzer. A typical three-electrode single compartment electrochemical cell included a glassy carbon (r = 1 mm) working electrode, a Ag^+/Ag reference electrode and a platinum wire auxiliary electrode in 10 mL of 0.1 M [n-Bu_4N][PF_6] as the supporting electrolyte. IR compensation for solution resistance was established prior to each measurement. Ferrocene was used as the internal standard ($E_{1/2}$ = 801 mV in THF versus NHE). Substrate concentrations were in the range of 5–20 mM. Melting points were taken with a Melt-Temp melting point apparatus. Elemental analyses were performed by Desert Analytics, Inc. Tucson AZ, or Atlantic Microlabs, Atlanta, GA.

2.2. Syntheses

*2.2.1. K[Ni(‘S_3’)CN] (K**1**, K**1-^{13}CN**)*

Sellmann and co-workers previously reported the preparation of the [NBu_4]**1** [23] and [NMe_4]**1** [18] salts of the anion [Ni(‘S_3’)CN]. The K salt was prepared and isolated as follows: potassium cyanide (0.145 g, 2.23 mmol) in 10 mL methanol and 1 mL H_2O was added to a stirring suspension of brown [Ni(‘S_3’)]$_2$ (0.685 g, 1.12 mmol) in 50 mL THF. The solution color changed from brown to yellow–brown with dissolution of the solids. Following 3 h of stirring, the solvent was removed in vacuo. The resulting solid was redissolved in 30 mL methanol yielding a tan precipitate that was removed by filtration through a medium porosity glass frit. The solvent was removed in vacuo and the brown solids were extracted with acetonitrile, filtered, and dried in vacuo. Trituration of the sticky brown solids with ethyl ether afforded a fine green powder that was collected by vacuum filtration. Yield: 0.553 g, 66%. ^1H NMR (d_6-acetone): δ 6.95 (t, C_6H_4, 2 H), 7.05 (t, C_6H_4, 2 H), 7.28 (d, C_6H_4, 2 H), 7.78 (d, C_6H_4, 2 H). ^{13}C NMR (d_6-acetone): δ 122.2 (C5–‘S_3’), 126.0 (Ni–^{13}CN), 128.3 (C4–‘S_3’), 128.8 (C3–‘S_3’), 130.1 (C6–‘S_3’), 133.3 (C1–‘S_3’), 156.3 (C2–‘S_3’). UV–Vis (THF), λ_{max} (ε, cm^{-1} M^{-1}): 290 (20 025), 318 (sh), 422 (1200), 628 (57). IR (KBr): ν_{CN} ($^{13}_{CN}$) = 2106 (2065) cm^{-1}. *Anal.* Calc. for $C_{13}H_8KNNiS_3$: C, 41.95; H, 2.16; N, 3.76. Found: C, 41.85; H, 2.44; N, 3.61%.

*2.2.2. Et_4N[Ni(‘S_3’)^{13}CN] (Et_4N**1–^{13}CN**)*

This complex was prepared following the literature procedure employing $K^{13}CN$ [18]. IR (KBr): (ν^{13}_{CN}) 2067 cm^{-1}. ^{13}C NMR (d_6-acetone): δ 122.2 (C5–‘S_3’), 124.7 (Ni–^{13}CN), 128.3 (C4–‘S_3’), 128.8 (C3–‘S_3’), 130.1 (C6–‘S_3’), 133.3 (C1–‘S_3’), 156.3 (C2–‘S_3’).

*2.2.3. (‘S_3’)Ni–CN–Fe[Tp^{tBu}](**2-Fe**)*

K**1** (0.060 g, 0.161 mmol) in 5 mL of THF was added dropwise to a stirring solution of [Tp^{tBu}]FeBr (0.084 g, 0.161 mmol) in 20 mL of THF. The resulting green–brown solution was to stirred overnight after which time a precipitate formed and the solution color changed to light brown. The solution was filtered through Celite and reduced to dryness in vacuo. The dry solid was washed with ethyl ether and a light brown solid was collected by filtration. X-ray quality crystals were grown by slow evaporation of concentrated benzene or THF solution. Yield: 0.076 g, 61%. ^1H NMR (C_6D_6): δ 67.4 (s, 4-pz), 29.5 (s, 5-pz), 18.4 (br, B–H), 9.5 (s, C_6H_4), 9.1 (s, C_6H_4), 8.3 (s, C_6H_4), 7.4 (s,C_6H_4), 3.3 (br, 3-pz-C(CH_3)$_3$). UV–Vis (THF), λ_{max} (ε, cm^{-1} M^{-1}): 262 (29 000), 290 (29 000), 320 (sh), 412 (1900), 640 (160). IR (KBr): (ν_{CN}) = 2120 cm^{-1}, (ν_{BH}) = 2493 cm^{-1}. μ_{eff} (solid, 294 K) = 5.4(1) μ_B. *Anal.* Calc. for $C_{34}H_{42}BFeN_7NiS_3$: C, 53.01; H, 5.49; N, 12.72. Found: C, 52.75; H, 5.20; N, 12.36%.

*2.2.4. (‘S_3’)Ni–CN–Co[Tp^{tBu}] (**2-Co**)*

To a stirring solution of [Tp^{tBu}]CoI (0.100 g 0.176 mmol) in 20 mL of THF was added K**1** (0.066 g 0.176 mmol) in 5 mL THF. The solution was stirred under N_2 overnight during which time the color changed from blue to dark green. The solution was filtered through Celite to remove the white precipitate (KI). The resulting deep green solution was dried in vacuo affording a green solid. X-ray quality crystals were grown by cooling a concentrated toluene solution to −25 °C for 48 h. Yield: 0.121 g, 89%. ^1H NMR (C_6D_6): δ 75.6 (s, 4-pz), 34.8 (s, 5-pz), 7.5 (s, C_6H_4), 7.3 (s, C_6H_4),

---

[1] Note added in proof: Following submission of this manuscript, a report of a Ni-CN-Fe complex appeared: D. Huang, L. Deng, J. Sun, R.H. Holm, Inorg. Chem 48 (2009) asap, doi:10.1021/ic900494u.

7.1 (br, 3-pz-C(CH_3)$_3$), 6.8 (s, C_6H_4), 6.3 (s, C_6H_4), −5.8 (br, B–*H*). UV–Vis (THF), λ_{max} (ε, cm^{-1} M^{-1}): 262 (28 000), 290 (29 000), 321 (sh), 405 (2500), 573 (970), 604 (1287), 623 (1337). IR (KBr): (ν_{CN}) = 2132 cm^{-1}, (ν_{BH}) = 2494 cm^{-1}. μ_{eff} (solid, 293 K) = 4.2(1) μ_B. *Anal.* Calc. for $C_{37.50}H_{46}BCoN_7NiS_3$: C, 54.96; H, 5.65; N, 11.96. Found: C, 54.40; H, 5.59; N, 12.16%.

2.2.5. *('S_3')Ni–CN–Ni[Tp^{tBu}]* (***2-Ni***)

K**1** (0.087 g, 0.236 mmol) in 10 mL of THF was added dropwise to a stirring solution of [Tp^{tBu}]NiCl (0.111 g, 0.236 mmol) in 10 mL of THF. The resulting solution was stirred for 6 h during which time the color turned dark red. The red solution was filtered through Celite and reduced to dryness in vacuo. The solid was washed with ethyl ether and a dark red product was collected by filtration. X-ray quality crystals were grown by evaporation of a concentrated 1,3,5-trimethylbenzene solution under a slow stream of N_2. Yield: 0.044 g, 25%. ^1H NMR (C_6D_6): δ 86.5 (s, 4-pz), 18.7 (s, 5-pz), −13.0 (br, B–*H*), 7.6 (s, C_6H_4), 7.4 (s, C_6H_4), 7.3 (s, C_6H_4), 7.1 (s,C_6H_4), 5.75 (br, 3-pz-C(CH_3)$_3$). UV–Vis (THF), λ_{max} (ε, cm^{-1} M^{-1}): 264 (14 500), 289 (18 000), 320 (sh), 409 (1300), 559 (270), 809 (67). IR (KBr): (ν_{CN}) = 2124 cm^{-1}, (ν_{BH}) = 2494 cm^{-1}. μ_{eff} (solid, 293 K) = 3.6(2) μ_B. *Anal.* Calc. for $C_{38.50}H_{48}BN_7Ni_2S_3$: C, 55.50; H, 5.80; N, 11.76. Found: C, 55.93; H, 5.80; N, 10.87%.

2.2.6. *('S_3')Ni–CN–Zn[Tp^{tBu}]* (***2-Zn***)

K**1** (0.077 g, 0.207 mmol) in 10 mL of THF was added dropwise to a stirring solution of [Tp^{tBu}]ZnCl (0.100 g, 0.207 mmol) in 20 mL of THF. The resulting brown colored solution was stirred overnight, then filtered through Celite and reduced to dryness in vacuo. The solid was extracted with 1,3,5-trimethylbenzene. The soluble material was isolated by filtration through Celite and dried in vacuo. X-ray quality crystals were grown by slow evaporation of a concentrated methylene chloride solution. Yield: 0.069 g, 43%. ^1H NMR (C_6D_6): δ 7.61 (d, C_6H_4, 2 H), 7.21 (d, C_6H_4, 2 H), 7.18 (s, 5-pz, 3 H), 6.79 (t, C_6H_4, 2 H), 6.59 (t, C_6H_4, 2 H), 5.69 (s, 4-pz, 3 H), 1.51 (s, 3-pz-C(CH_3)$_3$, 27 H). ^{13}C NMR (C_6D_6): δ 165.8 (3-pz), 154.8 (C2–'S_3'), 153.6 (Ni–^{13}CN–Zn), 136.6 (5-pz), 136.2 (C1–'S_3'), 133.2 (C6–'S_3'), 130.4 (C3–'S_3'), 129.0 (C4–'S_3'), 122.5 (C5–'S_3'), 103.0 (4-pz), 32.4 (*C*(CH_3)$_3$), 31.2 (C(CH_3)$_3$). UV–Vis (THF), λ_{max} (ε, cm^{-1} M^{-1}): 321 (sh), 400 (745). IR (KBr): $\nu_{CN,}$ (^{13}CN) = 2152, (2109) cm^{-1}, ν_{BH} 2494, (2497) cm^{-1}. *Anal.* Calc. for $C_{35}H_{44}BCl_2N_7NiS_3Zn$: C, 48.61; H, 5.13; N, 11.33. Found: C, 48.68; H, 5.36; N, 11.46%.

2.2.7. *[NEt_4][('S_3')Ni–CN–Cu(Tp^{tBu})]* (***2-Cu***)

NEt_4**1** (0.048 g, 0.103 mmol) in a 5 mL THF/CH_3CN (4:1) solution was added dropwise to a stirring solution of [Tp^{tBu}]Cu($NCCH_3$) (0.053 g, 0.110 mmol) in 20 mL THF. The orange solution was stirred for 8 h, filtered through Celite, and reduced to dryness in vacuo. The product was recrystallized by diffusion of pentane into a THF solution. Crystalline yield: 0.066 g, 70%. ^1H NMR (d_6-acetone): δ 7.82 (d, C_6H_4, 2 H), 7.36 (s, 5-pz, 3 H), 7.33 (d, C_6H_4, 2 H), 7.10 (t, C_6H_4, 2 H), 6.97 (t, C_6H_4, 2 H), 5.84 (d, 4-pz, 3 H), 3.39 (q, (CH_2CH_3)$_4$N, 8 H), 1.48 (s, 3-pz-C(CH_3)$_3$, 27 H), 1.31 (t, (CH_2CH_3)$_4$N, 12 H). ^{13}C NMR (d_6-acetone): δ 161.6 (3-pz), 156.5 (C2–'S_3'), 133.4 (5-pz), 133.2 (C1–'S_3'), 130.1 (C6–'S_3'), 128.9 (C3–'S_3'), 128.5 (Ni–^{13}CN–Cu), 128.3 (C4–'S_3'), 122.2 (C5–'S_3'), 100.1 (4-pz), 52.9 ((*C*H_2CH_3)$_4$N), 32.6 (*C*(CH_3)$_3$), 31.3 (C(CH_3)$_3$), 7.62 ((CH_2CH_3)$_4$N). UV–Vis (THF), λ_{max} (ε, cm^{-1} M^{-1}): 368 (sh), 419 (1681). IR (KBr): $\nu_{CN,}$ (ν^{13}_{CN}) = 2127, (2081) cm^{-1} (weak), ν_{BH} 2430, (2432) cm^{-1}. *Anal.* Calc. for $C_{42}H_{62}BCuN_8NiS_3$: C, 55.54; H, 6.88; N, 12.34. Found: C, 55.59; H, 6.95; N, 12.48%.

2.2.8. *Et_4N{[(^{2}-PhTt^{tBu})Cu]$_2$(μ-CN)}* ***3***

[NEt_4]CN (0.012 g, 0.076 mmol) was dissolved in 1 mL of acetonitrile and added to a stirring solution of [PhTt^{tBu}]Cu($NCCH_3$) (0.080 g,. 0.16 mmol) in 20 mL of acetonitrile. The solution was stirred overnight, filtered through Celite and the solvent was removed in vacuo. The off-white solid was extracted with THF, filtered through Celite and reduced to dryness under vacuum affording a white solid. Crystals were grown by vapor diffusion of pentane into a benzene solution or alternatively, by slow evaporation of concentrated acetonitrile solution. Crystalline Yield: 0.060 g, 75%. ^1H NMR (CD_3CN): δ 7.31 (s, *o*-(C_6H_5)B, 4 H), 7.04 (t, *m*-(C_6H_5), 4 H), 6.89 (t, *p*-(C_6H_5)B, 2 H), 3.13 (q, (CH_2CH_3)$_4$N, 8 H), 1.87 (s, CH_2B, 12 H), 1.29 (s, (C(CH_3)$_3$, 54 H), 1.18 (t, (CH_2CH_3)$_4$N, 12 H). ^{13}C NMR (CD_3CN): δ 132.9 ((*o*-C_6H_5)B), 127.4 ((*m*-C_6H_5)B), 124.2 ((*p*-C_6H_5)B), 53.0 ((CH_2CH_3)$_4$N), 43.7 (CH_2B), 30.2 (C(CH_3)$_3$), 7.75 ((CH_2CH_3)$_4$N). UV–Vis (THF), λ_{max} (ε, cm^{-1} M^{-1}): 220 (sh). IR (KBr): (ν_{CN}) = 2121 cm^{-1}. *Anal.* Calc. for $C_{51}H_{96}BCuN_2S_6$: C, 56.80; H, 8.97; N, 2.59. Found: C, 56.86; H, 8.68; N, 2.46%.

2.2.9. *[Tp^{tBu}]Zn^{13}CN*

This complex was prepared following the reported procedure [22] employing K^{13}CN. IR (KBr): (ν_{BH}) = 2526 cm^{-1}. ^{13}C NMR (C_6D_6): δ 30.92 (C(CH_3)$_3$, 32.1 (*C*(CH_3)$_3$, 102.5 (4-pz), 135.9 (5-pz), 137.7 (Zn–^{13}CN), 165.1 (3-pz).

2.3. *Density functional calculations*

Calculations were performed using GAUSSIAN03 [24]. Input atomic coordinates were derived from crystallographic determined structures. For computational expediency, the *tert*-butyl moieties of the Tp^{tBu} ligand were replaced with hydrogens. Molecular structures were optimized using the BLYP functional, Ahlrich's polarized triple-ζ quality basis set (TZVP) on zinc, nickel, copper, cyanide, sulfur, and the metal-bound pyrazolyl-nitrogen, and polarized split valence basis set on remaining atoms. Calculations using the BP86 method were also performed and yielded qualitatively similar results. Density fitting was employed and geometries were optimized to tight convergence criteria, which necessitated the use of tight SCF cutoffs and an ultrafine integration grid. To verify that each optimized structure was in fact a stationary point on the potential energy surface, analytical frequency calculations were performed, and no imaginary frequencies were obtained. Calculations aimed at the reliability of the wave functions with respect to open shell instabilities were also performed, and uncovered no lower energy solutions. Single point calculations were performed using the hybrid functional B3LYP with a balanced triple-ζ quality basis set, 6−311+g(d), on all atoms. The final energy was the sum of the electronic energy from the single point calculations and the thermal corrections from analytical frequency calculations at 298.15 K.

2.4. *X-ray crystallography*

X-ray structural analysis for **2-Fe**·0.5(thf), and **2-Zn**·(pentane): Crystals were mounted using viscous oil on glass fibers and cooled to the data collection temperature. Data were collected on a Bruker-AXS APEX CCD diffractometer with graphite-monochromated Mo-Kα radiation (λ = 0.71073 Å). Unit cell parameters were obtained from 60 data frames, 0.3° ω, from three different sections of the Ewald sphere. No symmetry higher than triclinic was observed for **2-Fe**·0.5(thf) and solution in the centrosymmetric space group option yielded chemically reasonable and computationally stable results of refinement. The systematic absences in the diffraction data are consistent with *Cmc*2$_1$ and *Cmcm* for **2-Zn**·(pentane). Only solution in the space group *Cmc*2$_1$ for **2-Zn**·(pentane) yielded chemically reasonable and computationally stable results of refinement. The absolute structure parameter refined to nil indicating that the true hand of the data for **Zn**·(pentane) had been determined. The data sets were treated with SADABS absorption corrections based on redundant multiscan data [25]. The structures were solved using direct methods and refined with full-matrix, least-squares procedures on F^2. Two symmetry unique but chemically identical compound molecules and one thf solvent molecule are located in the asymmetric unit of **2-Fe**·0.5(thf). The compound molecule lies on a mirror plane in **2-Zn**·(pentane). Disordered solvent molecules of crystallization were treated as diffused contributions [26]. Slight disorder, caused by the rotation of the *t*-butyl groups, which cannot be modeled because of the <1 Å difference in the disordered atomic positions, yielded less than optimal U_{eq} ranges. All non-hydrogen atoms were refined with anisotropic displacement parameters. All hydrogen atoms were treated as idealized contributions. Structure factors and anomalous dispersion coefficients are contained in the SHELXTL 6.12 program library [25]. The crystallographic details for isostructural compounds **2-Co**·2(toluene), **2-Ni**·0.5(mesitylene), **2-Zn**·2(CH_2Cl_2) and **2-Cu**·0.5(pentane)·(thf) are reported in the Supplementary material.

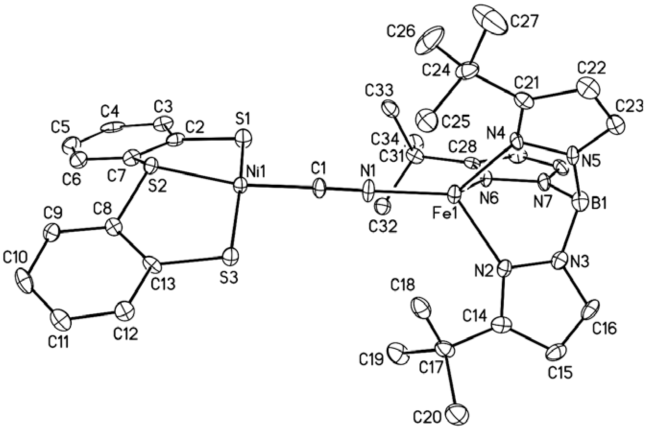

Fig. 1. Molecular structure of **2-Fe**. Thermal ellipsoids are drawn to 30% probability and hydrogen atoms have been omitted for clarity.

3. Results and discussion

3.1. Synthesis of cyanide-bridged binuclear complexes ***2-Fe***, ***2-Co***, ***2-Ni***, ***2-Zn***

The synthesis of a series of cyanide-bridged binuclear complexes proceeds by the coupling of two independently ligated metal complexes, Scheme 1. We chose the monoanion $[\mathrm{Ni(CN)('S_3')}]^-$, $\mathbf{1}^-$, ('S_3' = bis(2-mercaptophenyl)sulfide) first prepared by Sellmann et al. [18] due to its sulfur-rich ligation and square planar stereochemistry, the latter characteristic ensuring a diamagnetic complex. As emphasized by Holm is his recent studies [27], the Ni site in COdH has approximate square planar coordination despite being contained within the $NiFe_3S_4$ core. The nickel(II) ion is ligated by the tridentate thioether-dithiolate ligand ('S_3') and a cyanide ligand. The second portion of the cyanide-bridged complexes consists of the $[\mathrm{Tp^{tBu}}]$M fragment. The sterically demanding $[\mathrm{Tp^{tBu}}]$ ligand [19] allows for the isolation of monomeric metal halide complexes, $[\mathrm{Tp^{tBu}}]$MX, (M = Fe, Co, Ni, Zn; X = Cl, Br or I) as suitable precursors to the targeted binuclear complexes.

Initial attempts to synthesize the cyanide-bridged binuclear complexes using Et_4N**1** resulted only in recovery of the starting materials. Consequently, the synthetic protocol of Sellmann was altered to permit for isolation of K**1** reasoning that the potassium would add to the driving force of the coupling reaction via precipitation of KCl. Indeed, the room temperature reaction of K**1** with $[\mathrm{Tp^{tBu}}]$MX in THF produces the cyanide-bridged binuclear complexes ('S_3')Ni–CN–M$[\mathrm{Tp^{tBu}}]$ (M = Fe (**2-Fe**), Co (**2-Co**), Ni (**2-Ni**), Zn (**2-Zn**)) in variable yields. X-ray diffraction studies confirmed the formation of the isostructural series of binuclear cyanide-bridged complexes, *vide infra*.

3.2. X-ray structures of cyanide-bridged binuclear complexes **2**

A representative thermal ellipsoid plot (**2-Fe**) of the molecular structures of **2** is depicted in Fig. 1, and selected metric parameters summarized in Table 1. Plots of the isostructural complexes along with X-ray collection and refinement data are available in the Supplementary material. The general structural features of the complexes are quite similar, supporting the compositions and structures assigned based on spectroscopic evaluation, *vide infra*. The $[\mathrm{Tp^{tBu}}]$M fragment maintains its pseudo-tetrahedral geometry ligated to the linear cyanide bridge via the nitrogen atom. The cyanide is coordinated via the carbon atom to the square planar nickel ion. The M–NC distances fall within a very narrow range, decreasing across the period, from 1.980(2) Å for **2-Fe** to 1.925(2)/1.927(2) Å for **2-Zn**. The M–N bond lengths are consistent with the M^{2+} oxidation state assignment. The M–N–C and Ni–C–N angles are all within a few degrees, at most, to linear. The Ni–CN distances at ~1.850 Å, are insensitive of the identity of the second metal, whereas, the C–N distances fall within 1.135 to 1.163 Å, void of any apparent trends. The nickel 'S_3' coordination sphere is composed of two thiolate sulfur donors and one thioether sulfur donor with the tridentate ligand exhibiting a butterfly pucker as noted by Sellmann et al. [18] in which the thiolate sulfur atoms lie slightly below the idealized square plane and the thioether sulfur atom lies slightly above the plane.

3.3. Spectroscopy of cyanide-bridged binuclear complexes **2**

The room temperature proton NMR spectra of **2-Fe**, **2-Co** and **2-Ni** exhibit well dispersed paramagnetically-shifted signals for protons of the $[\mathrm{Tp^{tBu}}]$M fragments with the number of signals indicating three-fold symmetry of the ligand. The *t*-butyl groups of the $[\mathrm{Tp^{tBu}}]$ ligands appear as broad signals downfield of the diamagnetic ligand, $\delta = 3.3$ for **2-Fe**, 7.1 for **2-Co** and 5.7 for **2-Ni**. The 4-pz and 5-pz protons of the pyrazoyl rings and the B–H proton exhibit wide chemical shift dispersions, similar to those for analogous $[\mathrm{Tp^{tBu}}]$MX complexes. In each complex, the 'S_3' ligand displays four signals consistent with the mirror symmetry. Inter-

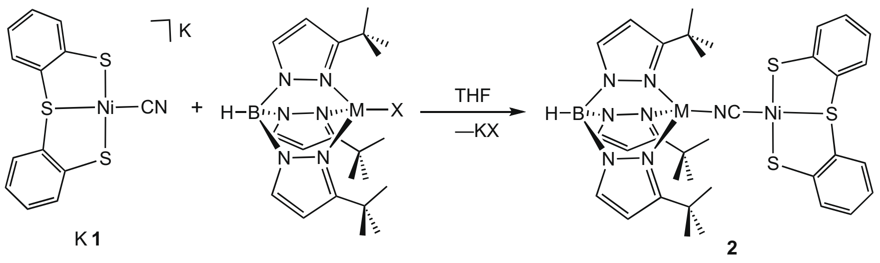

Scheme 1.

Table 1
Selected bond lengths (Å) and bond angles (°) for **2-Fe**, **2-Co**, **2-Ni**, **2-Zn**, and **2-Cu**.

2-Fe (2 independent molecules)	Length (Å)		Angle (°)
Fe1–N1	1.980(5)	Fe1–N1–C1	175.5(5)
Fe1–N_{pz} (avg)	2.064	Ni1–C1–N1	177.5(5)
Ni1–C1	1.850(6)		
Ni1–S1	2.181(2)		
Ni1–S2	2.110(2)		
Ni1–S3	2.159(2)		
C1–N1	1.145(7)		
Fe2–N8	1.980(5)		
Fe2–N_{pz} (avg)	2.057	Fe2–N8–C35	172.1(5)
Ni2–C35	1.850(6)	Ni2–C35–N8	178.1(6)
Ni2–S4	2.181(2)		
Ni2–S5	2.111(2)		
Ni2–S6	2.177(2)		
C35–N8	1.135(7)		
2-Co			
Co–N7	1.949(3)	Co–N7–C34	174.4(3)
Co–N_{pz} (avg)	2.014	Ni–C34–N7	179.1(3)
Ni–C34	1.846(3)		
Ni–S1	2.159(1)		
Ni–S2	2.106(1)		
Ni–S3	2.172(1)		
C34–N7	1.163(4)		
2-Ni			
Ni–N5	1.954(7)	Ni1–N5–C14	178.5(7)
Ni1– N_{pz} (avg)	1.992	Ni2–C14–N5	177.2(8)
Ni2–C14	1.842(8)		
Ni2–S1	2.174(2)		
Ni2–S1A	2.174(2)		
Ni2–S2	2.132(2)		
C14–N5	1.135(9)		
2-Zn *(2 independent molecules)*			
Zn1–N7	1.925(4)	Zn1–N7–C34	179.0(4)
Zn1–N_{pz} (avg)	2.018	Ni1–C34–N7	179.2(5)
Ni1–C34	1.850(4)		
Ni1–S1	2.159(1)		
Ni1–S2	2.131(1)		
Ni1–S3	2.179(1)		
C34–N7	1.135(6)		
Zn2–N14	1.927(4)	Zn2–N14–C68	174.8(4)
Zn2–N_{pz} (avg)	2.014	Ni2–C68–N14	176.3(5)
Ni2–C68	1.842(4)		
Ni2–S4	2.164(2)		
Ni2–S5	2.124(1)		
Ni2–S6	2.168(2)		
C68–N14	1.135(6)		
2-Cu			
Cu–N1	1.890(2)	Cu–N1–C13	177.8(2)
Cu–N_{pz} (avg)	2.100	Ni–C13–N1	178.8(2)
Ni–C13	1.856(2)		
Ni–S1	2.1685(8)		
Ni–S2	2.1108(7)		
Ni–S3	2.1814(8)		

estingly, in **2-Fe** these signals also exhibit small paramagnetic shifts. These slight downfield shifts are attributed to a through space dipolar shift interaction [28] caused by the paramagnetic iron. It is unlikely that a Fermi contact interaction is at the origin of the paramagnetic contributions to the phenyl proton chemical shifts due to the fact that the pathway through which spin could be delocalized is common amongst **2-Fe**, **2-Co**, and **2-Ni**. Specifically, in each complex, the magnetic orbitals are involved in cyanide binding, thus a Fermi contact shift would be expected for each complex. A dipolar shift mechanism is reasonable when considering (i) the smaller spin states of **2-Co** ($S = 3/2$) and **2-Ni** ($S = 1$) compared to **2-Fe** ($S = 2$) and (ii) the magnetic anisotropy as reflected in the molecular g-tensors, specifically, $g_{||}$, estimated at ~2.2 for **2-Ni** [29], 5.2 for **2-Co**, and ~8.5 for **2-Fe** [30]. The ^{1}H NMR spectrum of diamagnetic **2-Zn** is consistent with its structure as determined by X-ray diffraction.

The solid-state magnetic moments of solid samples of **2-Fe**, **2-Co** and **2-Ni** were determined using a magnetic susceptibility balance. In each case, the magnetic moment was consistent with the expected ground states as follows: **2-Fe**, $\mu_{eff} = 5.4(1)\ \mu_B$ for $S = 2$; **2-Co**, $\mu_{eff} = 4.2(1)\ \mu_B$ for $S = 3/2$; **2-Ni**, $\mu_{eff} = 3.6(2)\ \mu_B$ for $S = 1$.

The electronic absorption spectra of **2-Fe**, **2-Co**, **2-Ni** and **2-Zn** in THF displays two high energy Ni ← $S_{thiolate}$ and Ni ← $S_{thioether}$ ligand-to-metal charge transfer (LMCT) bands located at ca. 260 and 290 nm and a Ni ← CN metal-to-ligand charge transfer band (MLCT) at ~400 nm. These assignments are based on a comparison with the spectrum of the anion, [('S_3')Ni(CN)]$^-$, which displays nearly identical bands. The square planar nickel also displays a weak ligand field transition located at ~600 nm; this feature is observed in **2-Fe**, **2-Ni** and **2-Zn** [31]. In **2-Co** the Ni ligand field band is obscured by the Co ligand field transitions at 573, 604, and 623 nm, energies typical of tetrahedral cobalt(II) complexes [32]. **2-Ni** also displays two absorption features, located at 559 and 809 nm, assigned as ligand field transitions for the tetrahedral nickel site.

3.3.1. Infrared spectra of 2

Terminal M–CN linkages typically exhibit sharp, intense ν_{CN} modes between 2000 and 2200 cm^{-1} [33]. The ^{13}CN isotopically-labeled complexes were synthesized in order confirm spectral assignments and to address the issue of CN linkage isomerism in the bridged complexes as detailed later in this paper.

Upon formation of the cyanide-bridged complexes, the ν_{CN} frequency shifts to higher energy, Fig. 2 and Tables S3 and S4 (Supplementary material). The frequency shift ranges from 14–46 cm^{-1} depending on the identity of the metal ion with the order increasing, **2-Fe** < **2-Ni** < **2-Co** < **2-Zn**. Increases in ν_{CN} values for M–CN–M' compared with M–CN are well documented [5,33,34]. Typically the ν_{CN} increase has been rationalized as a consequence of the donation of σ-electron density from the antibonding lone pair on nitrogen. The depopulation of the antibonding orbital strengthens the CN triple bond, leading to an increase in ν_{CN} [1]. The kinematic effect [35], or the restraint of the CN group due to the attachment of a second mass, has also been offered to explain the observed

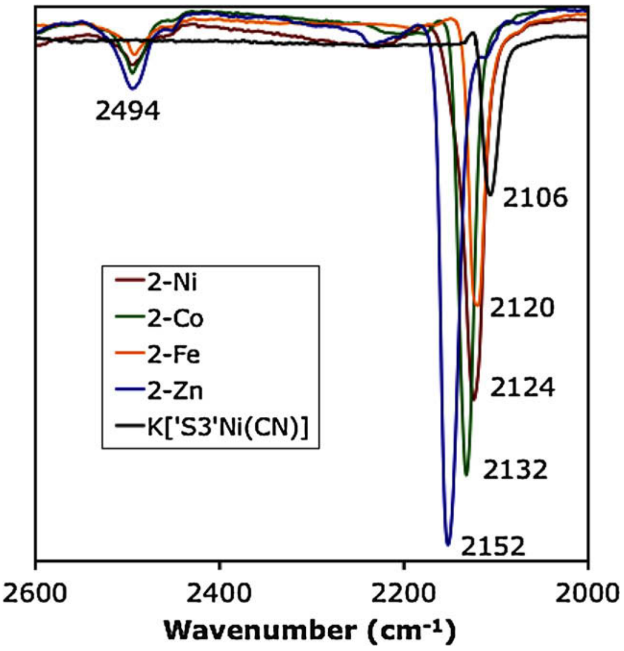

Fig. 2. Infrared spectra for the complexes K**1** and **2** in the 2000–2600 cm^{-1} frequency range.

increase of ν_{CN} in bridging complexes. However, a recent study has found that this effect has been overestimated and suggests that the kinematic effect does not contribute significantly to the observed ν_{CN} frequency increase [5]. In the present series of complexes, a correlation between the ν_{CN} value and M–N bond length is noted, wherein the complex with the shortest M–N bond length has the highest ν_{CN} value. This trend is consistent with the analysis above, as removal of electron density from the cyanide N lone pair strengthens the CN bond.

A number of factors can influence CN vibrational energy including metal oxidation state and C–N–M bond angle. Notable examples in biological systems include studies on COdH and cytochrome *c* oxidase. Infrared spectroscopic studies of COdH enzyme incubated with cyanide demonstrated a very low energy CN stretch at 2037 cm^{-1} [36]. It was postulated that the cause of the low energy vibration was due to carbon-bound cyanide coordination to a strongly π-donating metal (suggested to be Fe) in combination with a bent M–CN–M' bridge. Supporting the latter hypothesis, similarly low ν_{CN} energies were observed in synthetic models of an inhibited form of cytochrome *c* oxidase containing a Fe(III)–CN–Cu(II) linkage, with the frequency decreasing up to 60 cm^{-1} as the C–N–Cu bond angle decreased [34].

The ν_{BH} vibrational mode is sensitive to electronic changes in the metal coordination sphere and can be used to indicate binuclear complex formation. The ν_{BH} of the cyanide-bridged complexes shifts to lower energy as compared to the energy for the $[Tp^{tBu}]MX$ starting materials. Interestingly, the ν_{BH} value of ca. 2494 cm^{-1} is invariant among the complexes within the series. This significant change in stretching frequency upon bridge formation indicates that the $[(\text{'S}_3\text{'})Ni(CN)]^-$ fragment is a weaker σ-donor than the halide substituents of the $[Tp^{tBu}]MX$ precursors, resulting in reduction of negative charge at boron [37].

3.3.2. Electrochemical characterization of cyanide-bridged binuclear complexes **2**

Cyclic voltammetry experiments were conducted to establish the redox characteristics of the series of binuclear cyanide-bridged complexes. These electrochemical data are summarized in Table 2 (potentials referenced versus NHE). Each complex exhibits a quasi-reversible cathodic wave in the range ca. −1.0 to −1.2 V. Given the similarity among these complexes and with the monomeric precursor, $K[(\text{'S}_3\text{'})Ni(CN)]$, this feature is ascribed to the Ni(II)/Ni(I) couple of the square planar nickel site, although ('S_3') ligand-based reduction affords an alternative site to house the added electron. The CV of **2-Ni** displays a cathodic reduction wave at −0.96 V assigned as the Ni(II)/Ni(I) reduction for $[Tp^{tBu}]Ni$. For calibration, the reduction wave observed for $[Tp^{tBu}]NiCl$ is at −0.91 V. The reduction potential for the tetrahedral site in **2-Ni** is lower than the square planar ('S_3')Ni site due to the ability of the tetrahedral Ni site to support the Ni(I) oxidation state because of the lower energy of an available metal orbital (t_2-like symmetry) as compared to the higher energy LUMO ($d_{x^2-y^2}$) of the square planar site.

Table 2
Summary of CV data for K**1** and the series of complexes **2**.

	$E_{1/2}$, V Ni(II)/Ni(I)	I_{pa}/I_{pc}	E_{pc}, V
K**1**	−1.26	0.40	
2-Fe	−1.24	0.40	−2.02
		–	−2.33
2-Co	−1.25	0.21	−1.73
2-Ni	−1.18	0.11	−0.96
2-Zn	−0.91	0.54	–
	−1.21	0.15	–

Electrochemical experiments were performed in THF at a scan rate of 200 mV/s. Reduction potentials are referenced to internal Fc^+/Fc couple at +801 mV vs. NHE.

2-Co exhibits an irreversible cathodic wave at −1.73 V assigned to the Co(II)/Co(I) reduction based on comparison with $[Tp^{tBu}]CoI$. **3-Fe** exhibits two irreversible cathodic waves at −2.02 and −2.33 V, tentatively assigned as the Fe(II)/(I) and Fe(I)/Fe(0) reductions, respectively.

3.3.3. Mössbauer spectroscopy of **2-Fe**

The Mössbauer spectrum of **2-Fe** at 4.4 K in a magnetic field of 0.03 T exhibits a quadrupole doublet with an isomer shift, $\delta = 0.94(3)$ mm/s and quadrupole splitting $\Delta E_Q = 2.61(2)$ mm/s. The large isomer shift and quadrupole splitting are in the ranges corresponding to high-spin ferrous pseudo-tetrahedral species [38]. Mössbauer parameters of the C-cluster of COdH ferrous component II, FCII, (the unique iron) are $\Delta E_Q = 2.82$ mm/s and $\delta = 0.82$ mm/s [39], suggesting a pentacoordinate iron [40]. Interestingly, upon addition of cyanide to COdH, the quadrupole splitting changed to $\Delta E_Q = 2.53$ mm/s, while the isomer shift remained the same.

3.3.4. Electron paramagnetic resonance of **2-Co**

The EPR spectrum of **2-Co** recorded in toluene at 5 K exhibits a broad rhombic signal with effective *g*-values, $g = 5.3$, 4.2 and 2.2. These broad features are typical for high-spin, $S = 3/2$, tetrahedral cobalt(II) due to the ^{59}Co ($I = 7/2$) nuclear spin. Similar, broad EPR spectra have been reported for the mononuclear complex $[PhBP^{iPr}]CoI$ with $g \approx 4.8$ and $g \approx 2.2$ [41]. A similar EPR signal was reported for the cobalt substituted rubredoxin model complex $(Et_4N)_2[Co(SC_6H_4\text{-}p\text{-}Cl)_4]$ with effective *g*-values, $g = 4.8$, 3.6 and 2.08 [42].

3.4. Cyanide-bridged binuclear complex $Et_4N\{(\text{'S}_3\text{'})Ni\text{–}CN\text{–}Cu[Tp^{tBu}]\}$ **2-Cu**

Synthetic efforts to prepare the copper(II) cyanide-bridged binuclear complex commencing with $[Tp^{tBu}]CuCl$ proved unsuccessful. Thus, we turned to copper(I) precursors given the stability and established reactivity of copper(I) nitriles. The ionic complex $Et_4N\{(\text{'S}_3\text{'})Ni\text{–}CN\text{–}Cu[Tp^{tBu}]\}$, **2-Cu**, was isolated in good crystalline yield following the addition of Et_4N**1** to a THF solution of $[Tp^{tBu}]Cu(NCCH_3)$ [20] (Scheme 2).

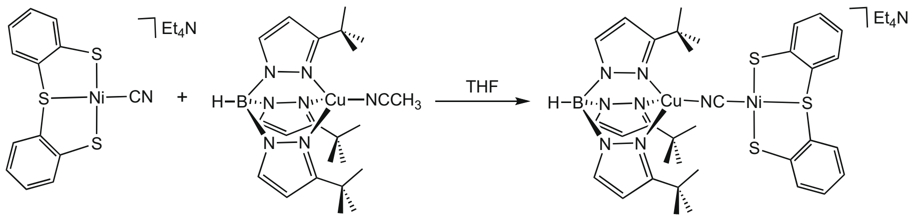

Et_4N**1**

2-Cu

Scheme 2.

3.4.1. X-ray structure of **2-Cu**

The molecular structure of the anion of **2-Cu**, which is isostructural with the other, neutral derivatives in this series is provided in the Supplementary material with selected metric parameters for the anion contained in Table 1. The copper coordination sphere is composed of three nitrogens from the $[Tp^{tBu}]$ ligand and a nitrogen of the cyanide ligand. The average Cu–N bond length from the nitrogen donors of the $[Tp^{tBu}]$ ligand is 2.100(2) Å, notably longer than the average Cu–N bond length of 2.064(5) Å in $[Tp^{iPr2}]Cu(NCCH_3)$ [43]. The Cu–NC distance is 1.890(2) Å, the shortest within the series of complexes reported here, and similar to the Cu–N bond of coordinated acetonitrile in $[Tp^{iPr2}]Cu(NCCH_3)$ at 1.875(6) Å. The Ni–CN–Cu linkage is linear. The square planar nickel(II) coordination sphere is composed of two thiolate sulfur donors at 2.1685(8) and 2.1814(8) Å and a thioether sulfur at 2.1108(7) Å. The fourth coordination site is occupied by the cyanide ligand with a Ni–C bond distance of 1.856(2) Å. The C–N bond length of the bridging cyanide ligand in **5** was found to be 1.148(3) Å, matching the C–N bond length of 1.153 Å in Me_4N**1** [18].

3.4.2. Spectroscopy of **2-Cu**

The electronic absorption spectrum of diamagnetic **2-Cu** in THF solution displays the bands of the nickel fragment: two high energy $Ni \leftarrow S_{thiolate}$ and $Ni \leftarrow S_{thioether}$ LMCT bands at 261 and 290 nm. An absorption feature at 419 (1680 $M^{-1}\,cm^{-1}$) nm is assigned to a $Ni \leftarrow CN$ MLCT as seen for the other complexes of this series.

The solid state IR spectrum of **2-Cu** displays a very weak ν_{CN} band at 2127 cm^{-1} and a ν_{BH} mode at 2429 cm^{-1}. The frequencies of these two modes are in accord with the frequencies for the neutral binuclear analogues. To confirm assignment of the unusually weak ν_{CN} mode, ^{13}CN-enriched **2-Cu–^{13}CN** was prepared. This sample displays a weak ν_{CN} mode at 2081 cm^{-1}; the shift in energy is in quantitative agreement with reduced mass considerations, i.e. ca. 2082 cm^{-1}. The unusually weak ν_{CN} signal intensity indicates a small dipole moment change associated with the vibration. As a consequence of the overall negative charge of **2-Cu** the charge distribution is such that the normally large CN dipole is significantly diminished. This assertion is supported by DFT calculations, *vide infra*.

The ^{13}C NMR spectrum of **2-Cu–^{13}CN** contains an intense singlet at $\delta = 128.5$, ascribed to the bridging ligand. Interestingly, this signal is shifted only slightly downfield of that for the enriched starting material, **Et_4N1–^{13}CN** at $\delta = 124.7$. In contrast, the ^{13}C NMR signal for **2-Zn–^{13}CN**, $\delta = 153.6$, exhibits a 28 ppm downfield shift indicating that in neutral **2-Zn** the cyanide carbon is significantly deshielded relative to the monomeric precursor. A similar downfield shift of the ^{13}C NMR resonance has been observed upon bridge formation in $(CO)_5W–CN–Cu(PPh_3)_3$, $\delta = 147.8$, relative to the anionic precursor, $Na[(CO)_5W(CN)]$, $\delta = 136.4$ [44]. As with the analysis of the intensity difference of the ν_{CN} bands, the charge distribution in the anion of **2-Cu** impacts this ^{13}C NMR spectral feature.

The cyclic voltammogram of **2-Cu** exhibits an irreversible Ni(II)/Ni(I) cathodic wave at −1.27 V, similar in value to this reduction in the neutral complexes. An irreversible anodic wave at 0.81 V is ascribed to the Cu(II)/Cu(I) couple. The irreversible electrochemical behavior indicates that upon oxidation to copper(II) **2-Cu** is unstable or undergoes a structural change. While it is perhaps surprising that the oxidized product is electrochemically unstable, this result is consistent with our inability to independently prepare the neutral Ni–CN–Cu(II) complex. A second irreversible anodic wave is located at 1.19 V is tentatively ascribed to ('S_3') ligand oxidation.

Table 3
Selected DFT optimized bond lengths and vibrational frequencies for the truncated model of **2-Cu**.

	$\{[(Tp)Cu]–NC–[Ni('S_3')]\}^{-1}$
C–N (Å)	1.1760
ν_{CN} (cm^{-1}) ([I])	2106.7 (3)
ν_{BH} (cm^{-1})	2448.6
$Ni–C_{CN}$ (Å)	1.8639
$Cu–N_{CN}$ (Å)	1.8994
$Cu–N_{Pz}$ (Å)	2.1437, 2.1523, 2.1579
$Ni–S_{trans}$ (Å)	2.1878

3.4.3. DFT analysis of **2-Cu**

DFT calculations were performed on **2-Cu** to clarify the unusually weak ν_{CN} intensity. In the computational model, the *tert*-butyl groups of the $[Tp^{tBu}]$ ligand were replaced with hydrogens, i.e. [Tp]. The optimized structure closely resembles the experimentally determined structure of **2-Cu** (Table 3). The key DFT derived vibrational bands, $\nu_{BH} = 2449\ cm^{-1}$ and $\nu_{CN} = 2107\ cm^{-1}$ are in good agreement with the experimental values, 2429 and 2127 cm^{-1}, respectively. The weak ν_{CN} intensity is reflected in part, in the value of the dipole moment of the anion. A comparison of the calculated dipole moments of **2-Cu** with **2-Zn** and its linkage isomer **2-Zn′** reveals a significantly lower dipole moment, $\mu = 1.6440$ D in the former compared to $\mu = 9.2796$ and 9.6028 D, in the latter two complexes. The correlation between the gas-phase DFT calculations and the experimental solid-state IR measurements indicates that this phenomenon is not a consequence of ion-pairing in the solid state.

3.5. Cyanide-bridged binuclear complex $Et_4N\{[(^2\text{-}PhTt^{tBu})Cu]_2\text{-}(\mu\text{-}CN)\}$ **3**

Following the preparation of cyanide-bridged binuclear complexes detailed in the preceding sections, efforts to extend this series of complexes using the tetrahedral metal precursors, $[PhTt^{tBu}]MCl$ ($PhTt^{tBu}$ = phenyl(tris(*tert*-butylthio)methyl)borate, M = Fe, Co, Ni, Zn) [45] in lieu of $[Tp^{tBu}]MX$ were investigated. These condensation reactions proved uniformly unsuccessful due, in part to lability of the $[PhTt^{tBu}]$ ligand under the reaction conditions. Subsequent synthetic efforts focused on the analogous reaction in Scheme 2, substituting the monovalent copper complex $[PhTt^{tBu}]Cu(NCCH_3)$ for $[Tp^{tBu}]Cu(NCCH_3)$. This reaction afforded unanticipated products, $Et_4N\{[(\kappa^2\text{-}PhTt^{tBu})Cu]_2(\mu\text{-}CN)\}$, **3**, and the known nickel dimer $[Ni('S_3')]_2$. The formation of **3** suggests that the copper(I) complex extracts cyanide from the nickel complex, perhaps via intermediacy of undetected $\{('S_3')NiCNCu[PhTt^{tBu}]\}^-$. The resulting ('$S_3$')Ni fragments couple yielding $[Ni('S_3')]_2$. The independent reaction of $[PhTt^{tBu}]Cu(NCCH_3)$ with half an equivalent of $[NEt_4]CN$ produces **3** in 75% yield.

3.5.1. Spectroscopy of **3**

The proton NMR spectrum of **3** in d_3-acetonitrile exhibited single *tert*-butyl and methylene proton resonances, $\delta = 1.29$ and 1.87, respectively, indicating magnetic equivalence of the thioether groups consistent with either symmetric ligation of the $[PhTt^{tBu}]$ ligand or that the thioether arms are in fast exchange on the NMR timescale. Such phenomena have been previously noted, for example in $[\kappa^2\text{-}PhTt^{tBu}]Ni(\eta^3\text{-allyl})$ [46].

Compound **3** exhibits a medium intensity $\nu_{CN} = 2121\ cm^{-1}$ for the bridging CN ligand. This band is similar in energy to the weak CN vibrational mode in the anionic **2-Cu** located at 2127 cm^{-1}, but with an intensity more characteristic of the other cyanide containing complexes.

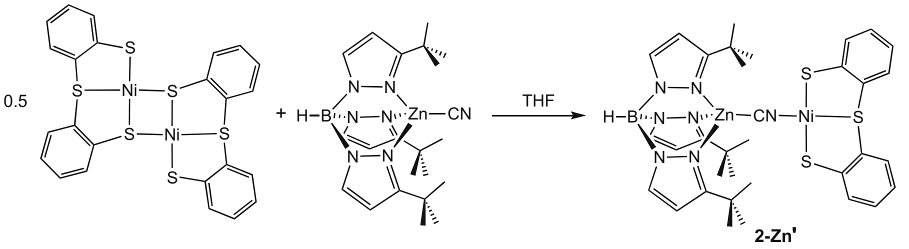

Scheme 3. Synthetic scheme for the (attempted) preparation of the CN linkage isomer, **2-Zn′**.

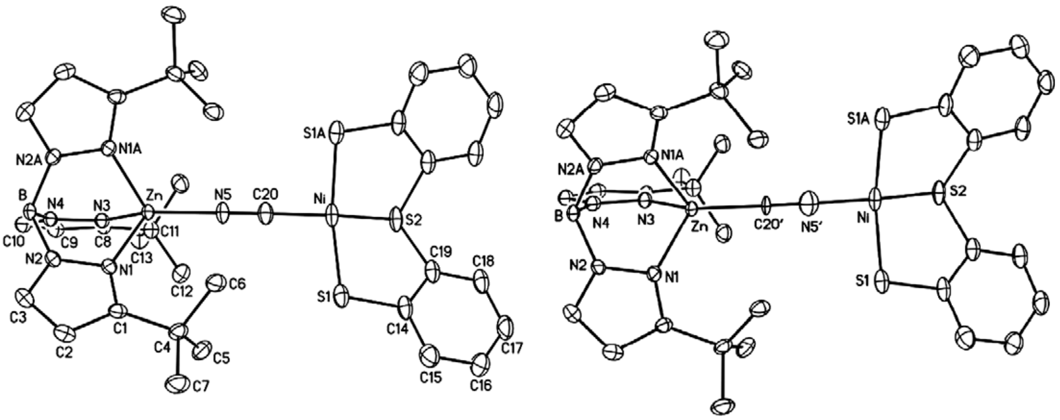

Fig. 3. Molecular structures of the proposed **2-Zn′** refined alternatively as the linkage isomers **2-Zn** (left) and **2-Zn′** (right) with thermal ellipsoids at 30%. Note the differences in the thermal ellipsoids of the cyanide ligands.

3.6. Cyanide linkage isomers

Here we describe efforts to assemble the cyanide-bridged linkage isomer of **2-Zn**, denoted as **2-Zn′**, for the purpose of establishing its structural and spectroscopic characteristics in comparison with **2-Zn**. The strategy for the synthesis of the series of cyanide-bridged binuclear complexes described above, highlights the approach of coupling of two metal complexes in which the cyanide ligand is affixed to one of the precursors. Implicit in this strategy is the assumption that under kinetic control, bridge formation proceeds without cyanide isomerization. With this consideration in mind, reaction of $[\mathrm{Tp}^{\mathrm{tBu}}]\mathrm{MCN}$ with $[\mathrm{Ni}(\text{‘S}_3\text{’})]_2$ should yield the corresponding isomer of **2** (at least under kinetic control). It is noted that the related trimer, $[\mathrm{Ni}(\text{‘S}_3\text{’})]_3$ undergoes facile bridge rupture in reactions with nucleophiles including KCN [23]. Very few four-coordinate tetrahedral metal complexes with terminal cyanide ligands have been reported and attempted syntheses in our laboratory have been largely unsuccessful. This reality limits the scope of this investigation. However, the application of known $[\mathrm{Tp}^{\mathrm{tBu}}]\mathrm{ZnCN}$ [22] permits us to test the validity of this approach (Scheme 3). As the NiZn binuclear complexes are diamagnetic, a direct comparison of the reaction products is amenable to NMR interrogation.

3.6.1. X-ray diffraction analyses

Addition of $[\mathrm{Tp}^{\mathrm{tBu}}]\mathrm{ZnCN}$ to suspension of $[\mathrm{Ni}(\text{‘S}_3\text{’})]_2$ in THF produced upon workup a brown solid in 48% yield. X-ray quality crystals were grown by slow diffusion of pentane into a concentrated 1,3,5-trimethylbenzene solution. The proposed **2-Zn′** material was recrystallized by pentane diffusion into concentrated mesitylene solution which yielded unsolvated crystals different from **2-Zn**$\cdot 2\mathrm{CH_2Cl_2}$. The molecule lies on a crystallographic mirror plane rendering each half of the complex metrically equivalent. The data set was alternatively modeled as the two isomers, **2-Zn** and **2-Zn′**, Fig. 3. The **2-Zn** model passed the Hirshfeld Rigid-Bond Test [47], which is a test for the agreement of thermal parameters for adjacent, bonded atoms. The **2-Zn′** model failed this test because the cyanide atoms (C20′ and N5′) were apparently misidentified. Nonetheless, while these data support isomerization to the **2-Zn** form, detailed spectroscopic studies were undertaken in effort to confirm the identity of this isomer.

3.6.2. Spectroscopic analyses

The proton NMR spectra of the products derived for the two independent synthetic routes are indistinguishable and do not warrant further description. Table 4 contains ^{13}C NMR and infrared spectroscopic data for the ^{13}CN labeled precursors and the products. The two products, **2-Zn** and proposed **2-Zn′**, exhibit identical ^{13}CN chemical shifts, $\delta = 153.3$. This result clearly supports the assertion that the products are identical. Further, the lack of a second cyanide signal rules out the possibility of compositional disor-

Table 4
IR and ^{13}C NMR spectroscopic data for K**1**, $[\mathrm{Tp}^{\mathrm{tBu}}]\mathrm{Zn}^{13}\mathrm{CN}$, **2-Zn** and the material proposed as **2-Zn′**.

	Experimental ν_{CN}, cm^{-1}	Calculated[a] $\nu_{13\mathrm{CN}}$, cm^{-1}	ν_{BH}, cm^{-1}	δ ^{13}CN
K**1**	2106	–	–	–
K**1-^{13}CN**	2065	2062	–	125.9
$[\mathrm{Tp}^{\mathrm{tBu}}]\mathrm{Zn}^{13}\mathrm{CN}$	2214[b]	–	2526	137.7
2-Zn	2152	–	2495	–
2-Zn–^{13}CN	2109	2107	2497	153.3
2-Zn′	2146	–	2493	–
2-Zn′–^{13}CN	2105	2103	2491	153.3

[a] Value calculated based on reduced mass differences assuming a simple diatomic oscillator.

[b] Ref. [49].

Table 5
Selected DFT optimized bond lengths and vibrational frequencies.

	(‘S_3’)Ni–NC–Zn[Tp]	(‘S_3’)Ni–CN–Zn[Tp]
C–N (Å)	1.16754	1.17742
ν_{CN} (cm^{-1}) ([I])	2176.0 (253)	2114.3 (1327)
ν_{BH} (cm^{-1})	2514.0	2514.7
Zn–C_{CN} (Å)	1.9580	n/a
Ni–N_{CN} (Å)	1.8637	n/a
Ni–C_{CN} (Å)	n/a	1.8309
Zn–N_{CN} (Å)	n/a	1.9083
Zn–N_{Pz} (Å)	2.0757, 2.0759, 2.0766	2.0706, 2.0706, 2.0711
Ni–S_{trans} (Å)	2.1630	2.1889

der (at least at concentrations detectable by NMR). In a relevant report of cyanide-bridged linkage isomers, Darensbourg and co-workers prepared $(CO)_5W–CN–Cu(PPh_3)_3$ and $(CO)_5W–NC–Cu(PPh_3)_3$ by two different synthetic routes, the products affording different spectral characteristics distinguishable by ^{13}C NMR spectroscopy [44]. The latter was found to undergo rearrangement in solution forming thermodynamically favored, $(CO)_5W–CN–Cu(PPh_3)_3$. Therefore, our ^{13}C NMR data indicate only **2-Zn** is generated here.

Solid-state IR spectra of the samples of **2-Zn** and proposed **2-Zn**′ (and their ^{13}CN labeled forms) exhibit ν_{CN} bands within four wavenumbers of one another, Table 4. The congruence of these values further suggests that the materials are identical. However, examples from the literature indicate that IR analysis of the ν_{CN} bands does not necessarily provide a compelling method for establishing cyanide-bridged linkages isomers. Notably, the two isomers $(CO)_5W–CN–Cu(PPh_3)_3$ and $(CO)_5W–NC–Cu(PPh_3)_3$, distinguishable by ^{13}C NMR spectroscopy, exhibit identical ν_{CN} stretching bands [44]. Alternatively, Vahrenkamp's $[Cp(CO)_2Fe–CN–Mn(CO)_2Cp]$ and $[Cp(CO)_2Fe–NC–Mn(CO)_2Cp]$ isomers display ν_{CN} modes that differ by 50 cm^{-1} [48]. The similar ν_{CN} frequencies for **2-Zn** and proposed **2-Zn**′ when considered with the X-ray and ^{13}C NMR data point to formation of a single isomer, **2-Zn**.

3.6.3. *DFT calculations of the linkage isomers, **2-Zn** and **2-Zn**′*

To further corroborate the experimental data indicating that the cyanide-bridged linkage isomer **2-Zn** is the thermodynamically more stable isomer, a computational study was undertaken. The computational models used [Tp] as a truncated version of [Tp^{tBu}]. The DFT optimized structures of the linkage isomers afforded overall slightly longer calculated bond distances compared to the X-ray crystallographic data (Table 5). The DFT optimized frequency analysis reveals that significant differences in ν_{CN} values are expected, with **2-Zn** ca. 46 cm^{-1} lower in energy. These results support the conclusion that a single product is formed from the two independent synthetic routes. Further, the **2-Zn** isomer is calculated to be 5 kcal/mol lower in energy.

4. Summary

A binuclear Ni–CN–Fe complex, **2-Fe**, designed to provide insight into the fundamental characteristics of the cyanide-inhibited form of the NiFeS enzyme COdH was spectroscopically and structurally characterized. The linear Ni–CN–Fe bridge displays a ν_{CN} value $\sim$80 cm^{-1} higher than that found in the inhibited form of COdH supporting the hypothesis that the bridge in the latter is bent. The scope of these studies was extended to include a series of isostructural cyanide-bridged binuclear complexes, **2-Co**, **2-Ni** and **2-Zn**. A similar coupling scheme was used to synthesize the copper(I) analogue, **2-Cu**, yielding the anionic complex. The copper analogue is isostructural with the neutral complexes as elucidated by spectroscopic and X-ray diffraction analysis. Interestingly, **2-Cu** did not exhibit an intense ν_{CN} stretching band. DFT computations reveal a significantly lower dipole moment for **2-Cu** than for the neutral **2-Zn** and **2-Zn**′ (and by extension **2-Fe**, **2-Co** and **2-Ni**). The lack of a significant dipole moment in the anion presumably translates to a small dipole moment change upon C–N stretching.

Two synthetic strategies were employed for the attempted synthesis of cyanide-bridged linkage isomers. The products of two different ^{13}CN labeled reactions intended to yield (‘S_3’)Ni–CN–Zn[Tp^{tBu}] and (‘S_3’)Ni–NC–Zn[Tp^{tBu}] were analyzed. The structural refinement of the proposed (‘S_3’)Ni–NC–Zn[Tp^{tBu}] complex exhibits a better structural refinement as (‘S_3’)Ni–CN–Zn[Tp^{tBu}]. This structural assignment was supported by the Hirshfeld Rigid-Bond Test [47] analysis, which clearly favored assignment as **2-Zn** over **2-Zn**′. Nearly identical infrared and ^{13}C NMR spectroscopic data provide additional evidence that (‘S_3’)Ni–CN–Zn[Tp^{tBu}] is produced in both reactions. DFT optimized structures of (‘S_3’)Ni–CN–Zn[Tp] and (‘S_3’)Ni–NC–Zn[Tp] suggest that (‘S_3’)Ni–CN–Zn[Tp] is the thermodynamically preferred structure by 5 kcal/mol supporting the formation of (‘S_3’)Ni–CN–Zn[Tp^{tBu}] by both synthetic routes.

Acknowledgements

These studies were supported by the NIH (GM59191). Computational resources used in these studies were provided in part by the Bioinformatics Center of the University of Arkansas for Medical Sciences (NIH Grant P20 RR-16460 from the IDeA Networks of Biomedical Research Excellence (INBRE) Program of the National Center for Research Resources). The Mössbauer spectrometer was purchased through NSF grant CHE-0421116 (to CVP).

Appendix A. Supplementary material

CCDC 718982, 718983, 718983, 718984, 718985, and 718986 contains the supplementary crystallographic data for [**2-Fe**·0.5(thf)], [**2-Co**·2(toluene)], [**2-Ni**·0.5(mesitylene)], (**2-Zn**), [**2-Zn**·(pentane)], and [**2-Cu**·0.5(pentane)·(thf)]. These data can be obtained free of charge from The Cambridge Crystallographic Data Centre via http://www.ccdc.cam.ac.uk/data_request/cif.

Supplementary data associated with this article can be found, in the online version, at doi:10.1016/j.ica.2009.05.042.

References

[1] K.R. Dunbar, R.A. Heintz, Prog. Inorg. Chem. 45 (1997) 283.

[2] G.N. Richardson, U. Brand, H. Vahrenkamp, Inorg. Chem. 38 (1999) 3070;
S.S. Kaye, J.R. Long, Catal. Today 120 (2007) 311.

[3] S. Ferlay, T. Mallah, R. Ouahes, P. Veillet, M. Verdaguer, Nature 378 (1995) 701.

[4] S.F.A. Kettle, G.L. Aschero, E. Diana, R. Rossetti, P.L. Stanghellini, Inorg. Chem. 45 (2006) 4928.

[5] S.F.A. Kettle, E. Diana, E. Boccaleri, P.L. Stanghellini, Inorg. Chem. 46 (2007) 2409.

[6] A. Volbeda, E. Garcia, C. Piras, A.L. Delacey, V.M. Fernandez, E.C. Hatchikian, M. Frey, J.C. Fontecilla-Camps, J. Am. Chem. Soc. 118 (1996) 12989;
J.W. Peters, W.N. Lanzilotta, B.J. Lemon, L.C. Seefeldt, Science 282 (1998) 1853.

[7] C.E. Cooper, G.C. Brown, J. Bioenerg. Biomembr. 40 (2008) 533.

[8] S.W. Ragsdale, J. Inorg. Biochem. 101 (2007) 1657;
C.G. Riordan, J. Biol. Inorg. Chem. 9 (2004) 542.

[9] C.L. Drennan, J.Y. Heo, M.D. Sintchak, E. Schreiter, P.W. Ludden, Proc. Natl. Acad. Sci. USA 98 (2001) 11973.

[10] H. Dobbek, V. Svetlitchnyi, L. Gremer, R. Huber, O. Meyer, Science 293 (2001) 1281.

[11] J.H. Joeung, H. Dobbek, Science 318 (2007) 1461.

[12] S.A. Ensign, M.R. Hyman, P.W. Ludden, Biochemistry 28 (1989) 4973;
M.E. Anderson, P.A. Lindahl, Biochemistry 33 (1994) 8702.

[13] J. Feng, P.A. Lindahl, J. Am. Chem. Soc. 126 (2004) 9094.

[14] V.J. DeRose, J. Telser, M.E. Anderson, P.A. Lindahl, B.M. Hoffman, J. Am. Chem. Soc. 120 (1998) 8767.

[15] D. Li, R. Clérac, G. Wang, G.T. Yee, S.M. Holmes, Eur. J. Inorg. Chem. (2007) 1341;
J.Z. Gu, L. Jiang, M.Y. Tan, T.B. Lu, J. Mol. Struct. 890 (2008) 24.

[16] D.F. Shriver, M.A. Drezdon, The Manipulation of Air Sensitive Compounds, second ed., Wiley, New York, 1986.

[17] A.B. Pangborn, M.A. Giardello, R.H. Grubbs, R.K. Rosen, F.J. Timmers, Organometallics 15 (1996) 1518.

[18] D. Sellmann, D. Häußinger, F.W. Heinemann, Eur. J. Inorg. Chem. (1999) 1715.

[19] S. Trofimenko, J.C. Calabrese, J.S. Thompson, Inorg. Chem. 26 (1987) 1507.

[20] S.M. Carrier, C.E. Ruggiero, W.B. Tolman, J. Am. Chem. Soc. 114 (1992) 4407.

[21] C. Ohrenberg, C.G. Riordan, L.M. Liable-Sands, A.L. Rheingold, Inorg. Chem. 40 (2001) 4276.

[22] K. Yoon, G. Parkin, Inorg. Chem. 31 (1992) 1656.

[23] D. Sellmann, F. Geipel, F.W. Heinemann, Chem. Eur. J. 6 (2000) 4279.

[24] R.C. Gaussian 03, M.J. Frisch, G.W. Trucks, H.B. Schlegel, G.E. Scuseria, M.A. Robb, J.R. Cheeseman, J.A. Montgomery Jr., T. Vreven, K.N. Kudin, J.C. Burant, J.M. Millam, S.S. Iyengar, J. Tomasi, V. Barone, B. Mennucci, M. Cossi, G. Scalmani, N. Rega, G.A. Petersson, H. Nakatsuji, M. Hada, M. Ehara, K. Toyota, R. Fukuda, J. Hasegawa, M. Ishida, T. Nakajima, Y. Honda, O. Kitao, H. Nakai, M. Klene, X. Li, J.E. Knox, H.P. Hratchian, J.B. Cross, V. Bakken, C. Adamo, J. Jaramillo, R. Gomperts, R.E. Stratmann, O. Yazyev, A.J. Austin, R. Cammi, C. Pomelli, J.W. Ochterski, P.Y. Ayala, K. Morokuma, G.A. Voth, P. Salvador, J.J. Dannenberg, V.G. Zakrzewski, S. Dapprich, A.D. Daniels, M.C. Strain, O. Farkas, D.K. Malick, A.D. Rabuck, K. Raghavachari, J.B. Foresman, J.V. Ortiz, Q. Cui, A.G. Baboul, S. Clifford, J. Cioslowski, B.B. Stefanov, G. Liu, A. Liashenko, P. Piskorz, I. Komaromi, R.L. Martin, D.J. Fox, T. Keith, M.A. Al-Laham, C.Y. Peng, A. Nanayakkara, M. Challacombe, P.M.W. Gill, B. Johnson, W. Chen, M.W. Wong, C. Gonzalez, J.A. Pople, Gaussian, Inc., Wallingford CT, 2004.

[25] G. Sheldrick, Bruker-AXS Inc., Madison, WI, 2001.

[26] A.L. Spek, J. Appl. Cryst. 36 (2003) 7.

[27] J. Sun, C. Tessier, R.H. Holm, Inorg. Chem. 46 (2007) 2691.

[28] L.-J. Ming, Nuclear magnetic resonance of paramagnetic metal centers in proteins, in: J. Larry Que (Ed.), Physical Methods in Bioinorganic Chemistry: Spectroscopy and Magnetism, University Science Books, Sausalito, CA, 2000, pp. 375–464.

[29] P.J. Desrochers, J. Telser, S.A. Zvyagin, A. Ozarowski, J. Krzystek, D.A. Vicic, Inorg. Chem. 45 (2006) 8930.

[30] E.G. Pavel, N. Kitajima, E.I. Solomon, J. Am. Chem. Soc. 120 (1998) 3949.

[31] F.A. Cotton, G. Wilkinson, C.A. Murillo, M. Bochmann, Advanced Inorganic Chemistry, sixth ed., John Wiley & Sons Inc., New York, 1999. p. 835.

[32] R.Y. Han, A. Looney, K. McNeill, G. Parkin, A.L. Rheingold, B.S. Haggerty, J. Inorg. Biochem. 49 (1993) 105.

[33] K. Nakamoto, Infrared and Raman Spectra of Inorganic and Coordination Compounds, fifth ed., John Wiley & Sons Inc., New York, 1997. Vol. B: Applications in Coordination, Organometallic and Bioinorganic Chemistry.

[34] M.J. Scott, R.H. Holm, J. Am. Chem. Soc. 116 (1994) 11357.

[35] D.A. Dows, A. Haim, W.K. Wilmarth, J. Inorg. Nucl. Chem. 21 (1961) 33.

[36] D. Qiu, M. Kumar, S.W. Ragsdale, T.G. Spiro, J. Am. Chem. Soc 118 (1996) 10429.

[37] S. Senda, Y. Ohki, T. Hirayama, D. Toda, J.-L. Chen, T. Matsumoto, H. Kawaguchi, K. Tatsumi, Inorg. Chem. 45 (2006) 9914.

[38] For recent examples, see: N. Muresan, C.N. Lu, M. Ghosh, J.C. Peters, M. Abe, L.M. Henling, T. Weyermoller, E. Bill, K. Wieghardt, Inorg. Chem. 47 (2008) 4579.

[39] Z. Hu, N.J. Spangler, M.E. Anderson, J. Xia, P.W. Ludden, P.A. Lindahl, E. Münck, J. Am. Chem. Soc. 118 (1996) 830.

[40] S. Ciurli, M. Carrie, J.A. Weigel, M.J. Carney, T.D.P. Stack, G.C. Papaefthymiou, R.H. Holm, J. Am. Chem. Soc. 112 (1990) 2654.

[41] T.A. Betley, J.C. Peters, Inorg. Chem. 42 (2003) 5074.

[42] K. Fukui, H. Ohya-Nishiguchi, N. Hirota, Bull. Chem. Soc. Jpn. 64 (1991) 1205.

[43] K. Fujisawa, T. Ono, Y. Ishikawa, N. Amir, Y. Miyashita, K. Okamoto, N. Lehnert, Inorg. Chem. 45 (2006) 1698.

[44] D.J. Darensbourg, J.C. Yoder, M.W. Holtcamp, K.K. Klausmeyer, J.H. Reibenspies, Inorg. Chem. 35 (1996) 4764.

[45] P.J. Schebler, C.G. Riordan, I. Guzei, A.L. Rheingold, Inorg. Chem. 37 (1998) 4754;
S.-J. Chiou, J. Innocent, K.-C. Lam, C.G. Riordan, L. Liable-Sands, A.L. Rheingold, Inorg. Chem. 39 (2000) 4347;
M.T. Mock, C.V. Popescu, G.P.A. Yap, W.G. Dougherty, C.G. Riordan, Inorg. Chem. 47 (2008) 1889.

[46] J.A. DuPont, M.B. Coxey, P.J. Schebler, C.D. Incarvito, W.G. Dougherty, G.P.A. Yap, A.L. Rheingold, C.G. Riordan, Organometallics 26 (2007) 971.

[47] F.L. Hirshfeld, Acta Crystallogr. A 32 (1976) 239.

[48] N.Y. Zhu, H. Vahrenkamp, Angew. Chem., Int. Ed. Engl. 33 (1994) 2090.

[49] A. Looney, R. Han, I.B. Gorrell, M. Cornebise, K. Yoon, G. Parkin, A.L. Rheingold, Organometallics 14 (1995) 274.